Background Pressure Effects on Ion Velocity Distributions in an SPT-100 Hall Thruster

Article *in* Journal of Propulsion and Power · January 2019

DOI: 10.2514/1.B37133

6 authors, including:

Natalia Macdonald
Air Force Research Laboratory
12 PUBLICATIONS **146** CITATIONS
SEE PROFILE

William A. Hargus
Air Force Research Laboratory, Edwards AFB, CA
169 PUBLICATIONS **2,265** CITATIONS
SEE PROFILE

JOURNAL OF PROPULSION AND POWER
Vol. 35, No. 2, March–April 2019

Background Pressure Effects on Ion Velocity Distributions in an SPT-100 Hall Thruster

Natalia MacDonald-Tenenbaum*
U.S. Air Force Research Laboratory, Edwards Air Force Base, California 93524
Quinn Pratt,† Michael Nakles,‡ and Nickolas Pilgram§
ERC, Inc., Edwards Air Force Base, California 93524
and
Michael Holmes¶ and William Hargus, Jr.**
U.S. Air Force Research Laboratory, Edwards Air Force Base, California 93524

DOI: 10.2514/1.B37133

Increased background pressure in vacuum chamber test facilities as compared to on-orbit operation has been shown to influence the operation of electric propulsion devices such as Hall thrusters. This study aims to elucidate the impact of pressure on the ionization and acceleration mechanisms in a stationary plasma thruster, model SPT-100 Hall thruster, using time-averaged and time-resolved laser-induced fluorescence velocimetry. The results are compared for the thruster operating at an applied 300 V (~4.25 A), with vacuum facility background pressures ranging from 1.7×10^{-5} to 8.0×10^{-5} torr. Time-averaged measurements reveal that, in general, an upstream shift in the position of the ionization and acceleration regions occurs as the facility pressure is increased above the nominal 1.7×10^{-5} torr. Time-resolved measurements, implemented using a sample-hold scheme with 1 μs resolution, emphasize that similar acceleration profiles are present within the Hall thruster discharge channel regardless of background pressure. Measurements taken at 3.5×10^{-5} torr, where the facility background neutral density is similar to the neutral density emitted from the thruster, unexpectedly show increased ion acceleration over the next highest pressure condition at 5.0×10^{-5} torr. These results indicate a not-yet well defined balance of the impacts of neutral ingestion, classical and turbulent electron transport on thruster operation, and that the ratio of the background to thruster neutral density is a more relevant benchmark than background pressure alone when evaluating Hall thruster operation.

I. Introduction

THE effects of the vacuum facility background pressure on a Hall thruster operation have been a topic garnering significant interest in recent years [1–6]. The guidelines for background pressure during ground testing for plume measurements, lifetime, and performance have been established for over two decades [7]. However, as the Hall thruster power and efficiency increase, a significant departure from predicted on-orbit operation based on ground test and simulation data has brought into question the validity of established pressure limits for thruster qualification. Typical pressures seen in research and development vacuum facilities during thruster operation are $\sim 1\text{–}5 \times 10^{-5}$ torr, with world-class test and evaluation facilities such as the NASA John H. Glenn Research Center's Vacuum Facility 5 approaching low 10^{-6} or middle 10^{-7} torr, depending on the propellant flow rate of the thruster [8]. Even these lower pressures are orders of magnitude higher than the less than 1×10^{-10} torr seen at geostationary orbit. It is therefore valuable to use various types of measurements to study how changing the background pressure impacts thruster operation in order to make well-informed extrapolations of ground test data to onorbit conditions and aid in the establishment of electric propulsion testing standards [9].

This paper seeks to isolate the effects of background pressure on ion acceleration within the channel and near-field plume of a stationary plasma thruster, model SPT-100. The SPT-100 is one of the most prolifically used Hall thrusters on the market, celebrating its 100th flight in August 2016. Manufactured by the Russian Experimental Design Bureau Fakel, the SPT-100 was made available to western satellite manufacturers beginning in the early 1990s for flight qualification. Early tests focused on confirming thruster performance and lifetime [10,11], followed by a series of studies investigating plume interactions with spacecraft components [12–14].

Studies by Manzella using emission spectroscopy [15] to estimate propellant ionization fraction and laser-induced fluorescence (LIF) [16] to measure ion velocity distributions were the first nonintrusive optical diagnostics applied to this thruster. Recent studies [17] have expanded on this work using LIF velocimetry for more extensive spatial and temporal mapping of axial and radial ion velocities throughout the plume of an SPT-100.

The results presented in this work describe LIF velocimetry of an SPT-100 Hall thruster operating with facility background pressures varying from 1.7×10^{-5} to 8.0×10^{-5} torr. Axial ion velocities are acquired from 16 mm inside the discharge channel to 50 mm into the near-field plume of the thruster along the channel centerline. Temporally and spatially resolved changes in the axial ion velocity are examined in order to provide insight into the dynamics of propellant ionization and acceleration in this thruster, as well as into how the plasmadynamics of the thruster are effected by background neutral ingestion and collisionality.

II. Experimental Apparatus

A. Chamber 3 Vacuum Facility

LIF measurements for this study are performed in Chamber 3 at the U.S. Air Force Research Laboratory (AFRL) at Edwards Air Force Base in California. Chamber 3 is a cylindrical, stainless steel vacuum

Received 18 May 2018; revision received 1 October 2018; accepted for publication 16 October 2018; published online Open Access 3 January 2019.

*Consultant; sasha.macdonald@gmail.com.
†Undergraduate Researcher, University of San Diego; quinn.t.pratt@gmail.com.
‡Reseacher; currently Aerospace Corporation; michael.naklesr@aero.org.
§Ph.D. Candidate, California Institute of Technology; npilgram1@gmail.com.
¶Research Scientist, In-Space Propulsion Branch; michael.holmes.23@us.af.mil.
**Research Engineer, Combustion Devices Branch; william.hargus@us.af.mil.

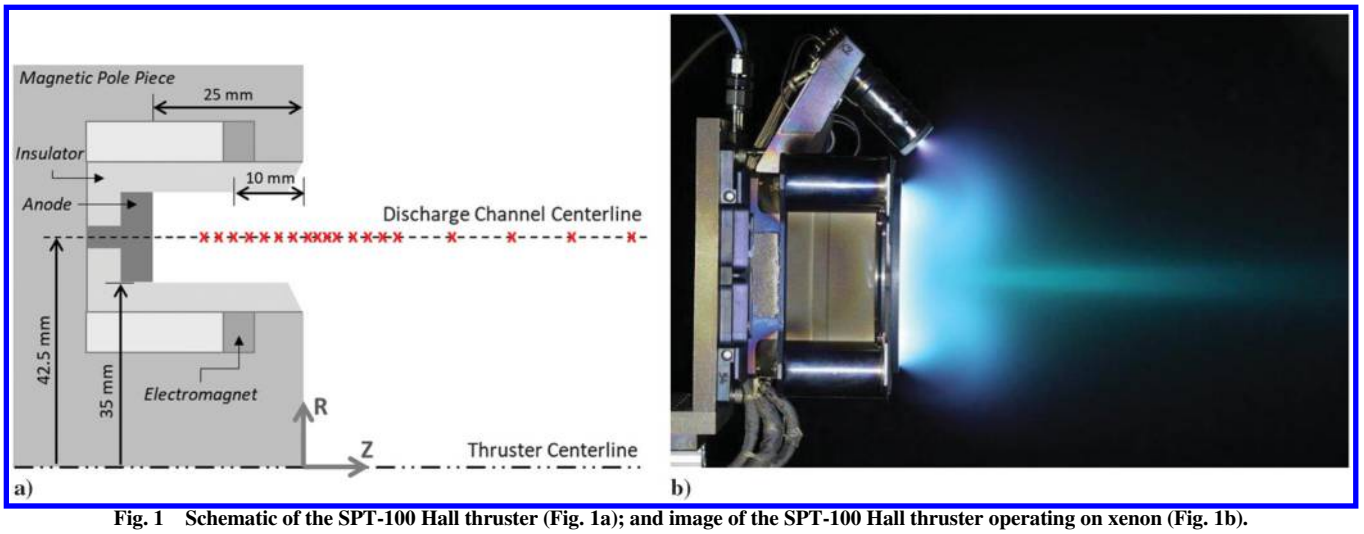

Fig. 1 Schematic of the SPT-100 Hall thruster (Fig. 1a); and image of the SPT-100 Hall thruster operating on xenon (Fig. 1b).

chamber that is 3.3 m in diameter and 8 m in length. The facility operates on eight helium-cooled cryopanels (20 K) backed by four IGC Polycold® cryogenic refrigeration units to provide a maximum xenon pumping speed of 140,000 l/s [18]. This facility is capable of achieving a background pressure of approximately 1.7×10^{-5} torr during nominal SPT-100 thruster operation. The facility background pressure is measured by an MKS Instruments cold cathode ionization gauge located on the chamber ceiling above the thruster. All pressures reported here have been corrected from indicated pressure using a gas sensitivity factor of 2.87 for xenon [19].

Research-grade xenon propellant (99.999% purity) is supplied to the thruster anode via a 1000 standard cm^3/min (sccm), Unit 1661 digital mass flow controller and to the cathode via a 100 sccm, Unit 8161 digital mass flow controller. For the high-pressure conditions in this study, an additional 48 to 160 sccm of xenon gas is flowed into the chamber via a gas feedthrough located approximately 1 m below the exit plane of the thruster in order to achieve background pressures of 3.5×10^{-5} to 8.0×10^{-5} torr. This auxiliary flow line is regulated by an additional 1000 sccm, Unit 1661 digital mass flow controller, allowing for a more repeatable and stable method of raising the background pressure than would be accomplished by turning off individual cryopumps [3].

B. SPT-100 Hall Thruster

Figure 1 provides a schematic of the SPT-100 Hall thruster and an image of the SPT-100 operating on xenon. The measurements presented in this paper were taken at 22 spatial points from −16 mm inside the thruster discharge channel to +50 mm into the near field plume, as indicated on the thruster schematic.

The operating conditions for this study are outlined in Table 1. The nominal condition was chosen to match the applied discharge voltage and anode mass flow rate during previous testing of the SPT-100 at the AFRL [20]. The overall setpoint of the thruster had a slightly lower discharge current than in previous testing due to various factors including extensive operation of the available thruster before use in this study (greater than 200 h), use of laboratory power supplies and mass flow controllers rather than flight model equipment, and operation in a different vacuum chamber (Chamber 1 at the AFRL, which is smaller and operates at higher background pressure).

Typical discharge current characteristics of the SPT-100 are shown in Fig. 2a for the thruster operating at 1.7×10^{-5} and 8.0×10^{-5} torr (the lowest- and highest-pressure operating conditions). Fast Fourier transfers (FFTs) of the discharge current at all five operating conditions are provided in Fig. 2b. These traces show that, at the nominal operating pressure of 1.7×10^{-5} torr, the thruster oscillates quasi periodically at a frequency of 19.8 ± 5.24 kHz, resulting in a typical current cycle with a period of 50.3 ± 14.7 μs. At increasing pressures, the thruster oscillations increase in frequency, becoming more periodic (i.e., having narrower FFTs). At 8.0×10^{-5} torr, the discharge current frequency is 26.5 ± 1.68 kHz, resulting in a typical current cycle with a period of 37.8 ± 2.41 μs. These changes in discharge current oscillation frequency with pressure are consistent with recent observations in several other Hall thrusters [3,21].

C. Laser-Induced Fluorescence Velocimetry

Ion velocity measurements are accomplished by probing the $5d[4]_{7/2} - 6p[3]_{5/2}$ electronic transition of the xenon ion, Xe II, at 834.72 nm (air). The upper state of this transition is shared by the $6s[2]_{3/2} - 6p[3]_{5/2}$ transition at 541.92 nm [19], whichis used for the nonresonant fluorescence collection. This transition has been used extensively throughout the electric propulsion community for time-averaged and time-resolved LIF velocimetry [16,22–24].

Figure 3 depicts the optical train and associated equipment used in this experiment [17,25]. A New Focus Vortex TLB-6917 tunable diode laser is used to seed a TA-7600 VAMP tapered amplifier to achieve a probe beam output power of 82 mW. A saturation study was done prior to taking the measurements presented in this work, verifying that this laser power was well within the linear regime.

Beam pickoffs send portions of the beam into a Fabry–Perot (F-P) etalon for frequency reference and an optogalvanic xenon reference

Table 1 SPT-100 Hall thruster operating conditions

Background pressure	1.7×10^{-5} torr	3.5×10^{-5} torr	5.0×10^{-5} torr	6.5×10^{-5} torr	8.0×10^{-5} torr
Injected gas flow	None	4.72 mg/s Xe (48.0 sccm)	7.67 mg/s Xe (78.0 sccm)	11.8 mg/s Xe (120 sccm)	15.7 mg/s Xe (160 sccm)
Anode flow	5.16 mg/s Xe (52.5 sccm)	5.16 mg/s Xe (52.5 sccm)	5.16 mg/s Xe (52.5 sccm)	5.16 mg/s Xe (52.5 sccm)	5.16 mg/s Xe (52.5 sccm)
Cathode flow	0.396 mg/s Xe (4.03 sccm)	0.396 mg/s Xe (4.03 sccm)	0.396 mg/s Xe (4.03 sccm)	0.396 mg/s Xe (4.03 sccm)	0.396 mg/s Xe (4.03 sccm)
Anode potential, V	300	300	300	300	300
Anode current, A	4.24	4.24	4.25	4.26	4.28
Discharge frequency, kHz	19.8 ± 5.24	23.8 ± 4.31	24.5 ± 2.65	25.4 ± 1.99	26.5 ± 1.68

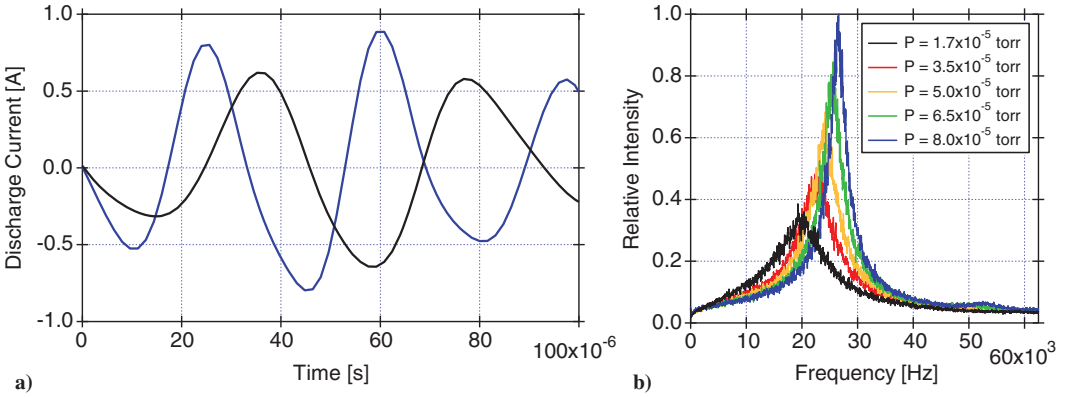

Fig. 2 Thruster discharge current at 1.7×10^{-5} torr and 8.0×10^{-5} torr (Fig. 2a); and associated FFTs for the operating conditions in Table 1 (Fig. 2b).

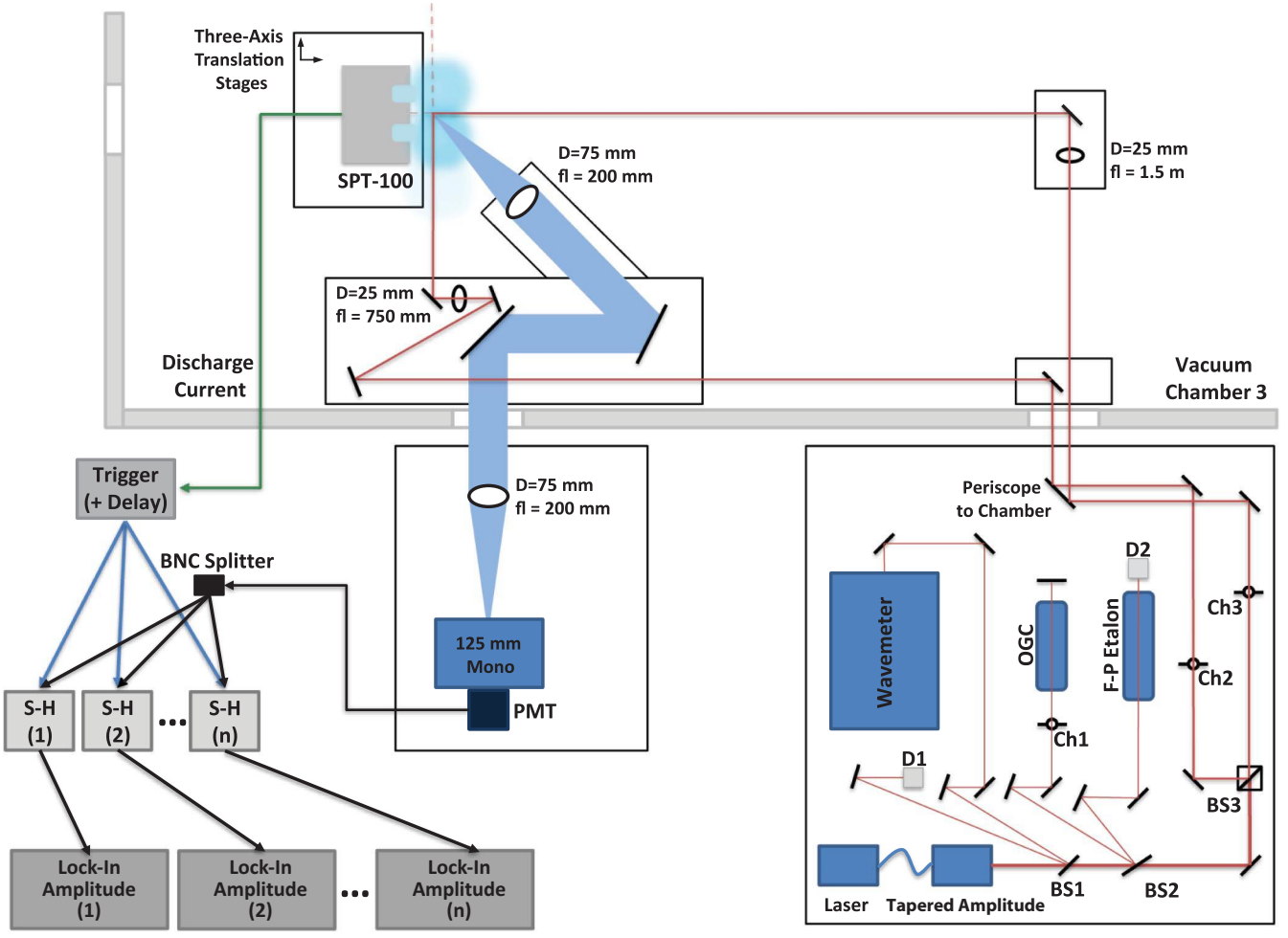

Fig. 3 Laser optical train, including launch and collection optics, and parallelized sample-hold scheme.

cell (OGC) for a zero-velocity spectral line reference. Homodyne detection allows us to probe the 9.03 GHz distant $6p'[3/2]_1 - 8s'[3/2]_1$ Xe I neutral transition in the OGC [26–28]. A typical 30 GHz laser scan is accomplished in ~8 min with a lock-in time constant of 3 s.

The majority of the probe beam (~68 mW) is sent through a beam splitter (BS3) to divide it into axial and radial components going through separate choppers before entering the vacuum chamber. The fluorescence induced by both the axial and radial probe beams is collected at a 45 deg angle from the probe beam axis using a 200 mm focal length lens with a 75 mm diameter. The collimated fluorescence signal is directed through a window in the chamber sidewall to a similar lens that focuses the collected fluorescence onto the entrance slit of the 125 mm focal length monochromator attached to a photomultiplier tube (PMT). The collection optics have a 1:1 magnification, which allows the spatial resolution of the measurements to be determined by the diameter of the probe beam (greater than 1 mm) and the image of the entrance slit (1.0 mm width by 1.7 mm height) that defines the collection optics solid angle. Choppers (Ch1 = 1.9 kHz, Ch2 = 2.5 kHz, and Ch3 = 3.2 kHz) are used for homodyne detection of the OGC, and the radial and axial fluorescence signals, respectively. For the axial and radial beams, the resulting signal is a time-averaged measurement of the fluorescence excitation line shape if the PMT signal is sent directly into a lock-in amplifier. For this background pressure study, only axial ion velocity measurements are presented. The results of the radial ion velocity measurements at the nominal background pressure are provided elsewhere [17].

To achieve a time-resolved LIF measurement, a sample-hold scheme is implemented between the PMT and the lock-in amplifier to synchronize the acquisition of fluorescence excitation line shapes to the discharge current oscillations. The development of this sample-hold scheme is described elsewhere [28–30]. The basis of the sample-hold method is to trigger an acquisition gate at various phases of the discharge current oscillation period of the thruster, during which the PMT signal (emission plus fluorescence) is sampled, averaged, and held until the next trigger, at which point, the held signal is updated (once per period). The gate width chosen for this study is 1 μs to allow for multiple points of time resolution throughout the discharge current cycle. The sample-held signal is then sent through a lock-in amplifier for homodyne detection, resulting in a fluorescence excitation line shape representing the ion velocity distribution function (IVDF) at that particular phase of the discharge oscillation. To reduce data acquisition time, the sample-hold circuitry (labeled S-H in Fig. 3) in his work is parallelized by splitting the PMT signal into several sample-hold branches, with each triggered at different phases in the discharge current cycle with a 1 μs gate width, as shown in Fig. 3. The use of seven lock-in seven lock-in amplifiers enabled measurements of IVDFs at seven temporal points during a single laser scan, for up to 21 points of time resolution in a typical set of three laser scans.

It is of note that, due to the quasi-periodic naturally drifting current oscillations in the SPT-100, the acquisition gate width is smaller than the ± 2.41 to 14.7 μs fluctuation in the discharge current period (for the 8.0×10^{-5} and 1.7×10^{-5} torr conditions, respectively). This introduces some uncertainty in the time-resolved measurements in terms of sampling at phases earlier or later in the discharge current cycle than desired, resulting in some time averaging between nearby phases that makes our time-resolved results more homogeneous than we have seen in thrusters with more periodic discharge current cycles,

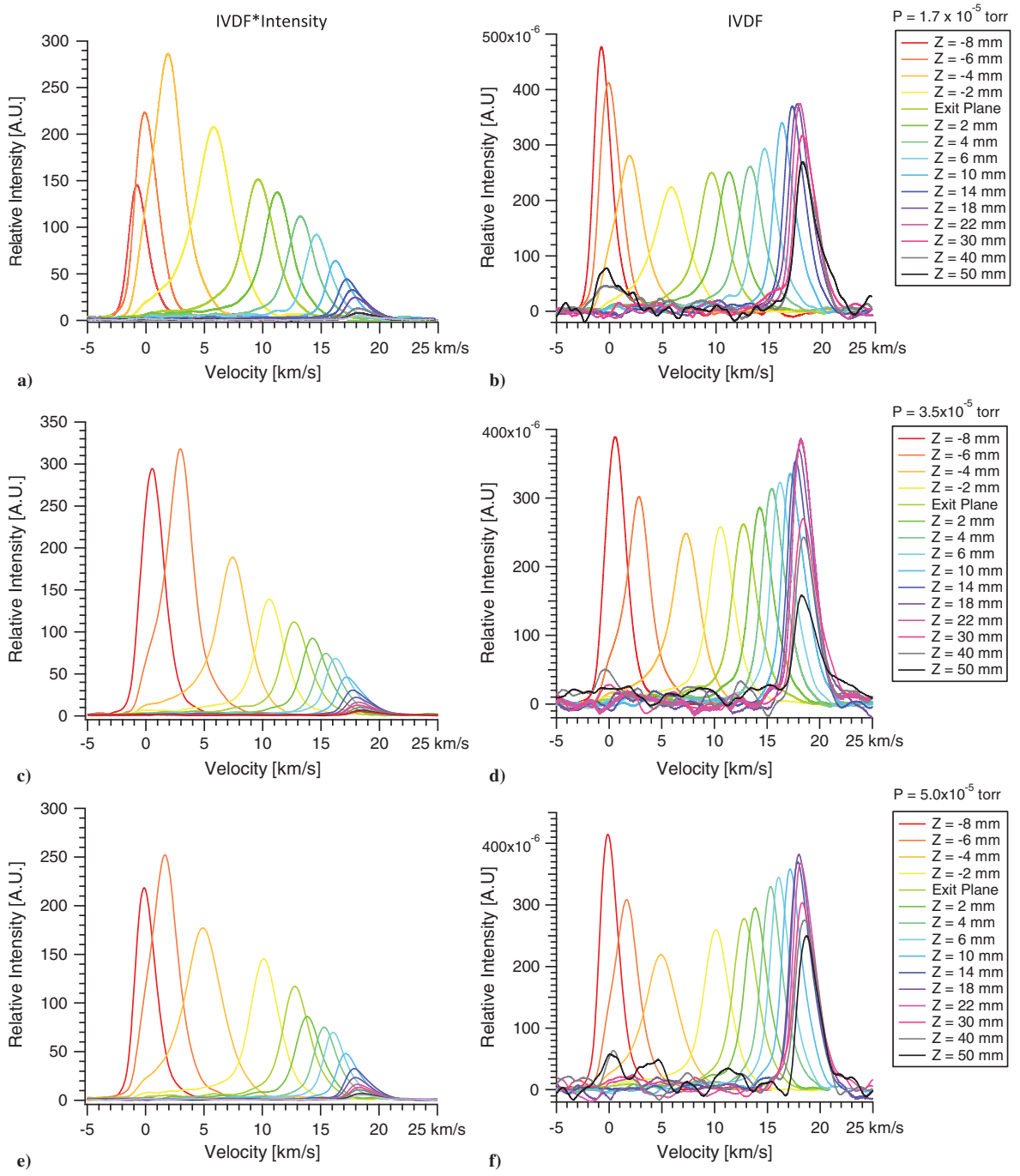

Fig. 4 Time-averaged axial IVDFs: fluorescence excitation line shapes in which relative intensity scales with density of the probed excited state (left), and IVDF normalized for unity area (right).

such as the BHT-600 [28]. Previous work has sought to quantify this temporal uncertainty [31]. The velocities presented in this study are estimated to have a ±500 m/s absolute accuracy based mainly on the uncertainty in the location of the $6p'[3/2]_1 - 8s'[3/2]_1$ Xe I reference transition. The precision (or repeatability) of the measurements is ±100 m/s.

III. Results and Discussion

The results in this work are analyzed and presented in three ways. First, we present fluorescence excitation line shapes, which are a representation of IVDFs scaled by the measured fluorescence intensity. Second, the measured fluorescence excitation line shapes are normalized such that the area under each distribution is unity. In this way, we determine the IVDFs. Finally, the most probable velocities are determined by measuring the peaks of the IVDFs.

The process to analyze these measurements begins with scaling the measured line shapes on the x axis to velocity space using the Doppler shift relationship and the etalon trace to mark the frequency spacing to the stationary reference signal from the OGC. Each fluorescence excitation line shape represents the convolution of the IVDF, the spectral transition line shape, the probe laser line shape, and instrument broadening at a given spatial position. Previous studies have shown that Doppler broadening is dominant in this type of plasma discharge, allowing us to take the measured line shape as a velocity distribution with little increase in error [32].

The relative intensity of the fluorescence excitation line shapes is representative of the population of ions in the probed metastable Xe II excited state ($5d[4]_{7/2}$) within the collection volume. This population is tied to the Xe II ground state via a combination of electron impact ionization and excitation, radiative decay, and local electron and ion transport mechanisms [33]. The measured intensity has previously been used as an indication of the ion population [28], which is a good assumption when looking at the time variation of IVDFs at a given point in the discharge. It is of note that any comparison of intensities at different points along the discharge channel is subject to variations in properties such as local electron temperature; therefore, these observations are more qualitative in nature.

A. Time-Averaged Measurements

Figure 4 provides the time-averaged axial ion velocity distributions in the SPT-100 operating at pressures of $P = 1.7 \times 10^{-5}$, 3.5×10^{-5}, and 5.0×10^{-5} torr. The left-hand column represents the fluorescence excitation line shapes from positions −8 mm inside the thruster discharge channel to +50 mm into the near-field plume. In Fig. 4a, the ion velocity at 1.7×10^{-5} torr starts out slightly negative (∼ − 800 m/s). Negative velocities at positions close to the anode have previously been attributed to a gradient-driven field reversal [34–36]. For the 3.5×10^{-5} and 5.0×10^{-5} torr cases, negative velocities are seen closer to the anode at $Z = -12$ and −16 mm, but these traces have been omitted from the figure due to a much lower S/N that would obscure other portions of the plot.

As the velocities increase, so does the amplitude of the fluorescence excitation line shape, building in intensity until a maximum at $Z = -4$ mm. This maximum intensity likely represents a region of peak ionization. Figures 4c and 4e show that, at elevated background pressure, the location of peak ionization is shifted upstream toward the anode: in both cases, measured at $Z = -6$ mm. At all three pressure conditions, the amplitudes of the fluorescence excitation line shape then fall off exponentially as velocity increases outward into the plume.

Focusing on the IVDFs in Figs. 4b, 4d, and 4f, the distributions start out narrow and Gaussian in shape, potentially due to thermalization of the ions. The IVDFs just after the previously noted locations of peak intensity become much broader, with significant low-velocity tails extending toward zero. The probed volume in this region is likely comprised of ions originating at different positions within the discharge channel, having experienced varying amounts of potential drop depending on the phase of the breathing mode cycle in which they are ionized (due to time-varying local potential fields) [28]. The IVDFs continue to narrow as the peak velocities increase, with diminishing low-velocity tails until ∼18 to 22 mm into the plume. After these positions, the primary velocity peaks decrease in amplitude as their peak positions in velocity space asymptote to ∼18.1 km/s, and distinct secondary velocity distributions appear near zero velocity. This pattern is similar for all three pressure conditions, but it is most noticeable in Figs. 4b and 4f. It is likely that these zero-velocity ions are born through charge exchange collisions with background neutrals. Previous work has estimated the collisional cross section for Xe–Xe^+ charge exchange as more than an order of magnitude greater than the next most significant collisional process of Xe–Xe^+ momentum exchange [7,37].

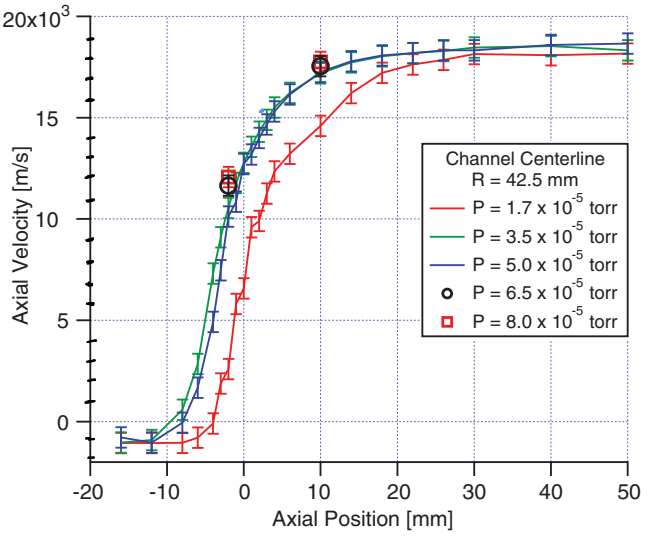

Fig. 5 Variation in time-averaged most probable axial velocity along the discharge channel of the SPT-100 Hall thruster operating at various vacuum chamber background pressures.

Figure 5 summarizes the most probable ion velocities along the centerline of the thruster channel for the three pressures reported in Fig. 4, with the addition of measurements at pressures of 6.5×10^{-5} and 8.0×10^{-5} torr, which were taken only at a subset of axial positions ($Z = -2$ and +10 mm). As was previously noted, this figure indicates that raising the vacuum chamber background pressure tends to shift axial ion acceleration upstream toward the anode. The largest jump in position (∼3 mm) occurs between the 1.7×10^{-5} and 3.5×10^{-5} torr cases. Between $Z = -12$ and the exit plane, the 3.5×10^{-5} torr condition accelerates ions ∼1 mm earlier than the 5.0×10^{-5} torr case, which is unexpected. The velocity differences appear to be repeatable and outside our measurement uncertainty, indicating that there may be some phenomena at this pressure that needs further investigation.

The ultimate ion velocity achieved of ∼18.1 km/s at positions outward of 30 mm into the near-field plume appears unaffected by background pressure. This result indicates that variations in background pressure affect the location but not the total extent to which the ions are accelerated by the applied potential drop.

Figure 6 compares the IVDFs for the various background pressures at several axial positions in the plume. Figure 5 is repeated in Fig. 6f for reference, with the IVDFs at each indicated point matching the same color scheme for varying pressures. In Fig. 6a, we see that ions at 1.7×10^{-5} torr have not yet begun accelerating at $Z = -6$ mm. This is compared to the higher pressures at which a much smaller fraction of ions remain near zero velocity, and high-velocity tails reaching past 5 km/s are more prominent.

At $Z = -4$ mm, shown in Fig. 6b, the largest variation is seen between the three distributions. As previously noted, it is undetermined why the 3.5×10^{-5} torr case has accelerated past the 5.0×10^{-5} torr case at this point. Considering that $Z = -4$ mm is a point of peak ionization for the higher-pressure conditions, this may be a region of the thruster where the interplay between ions and neutral propellant or ingested background gas is particularly complex.

A study by Crofton et al. on an SPT-140 Hall thruster [38] (a similar but higher-powered version of the SPT-100) showed that

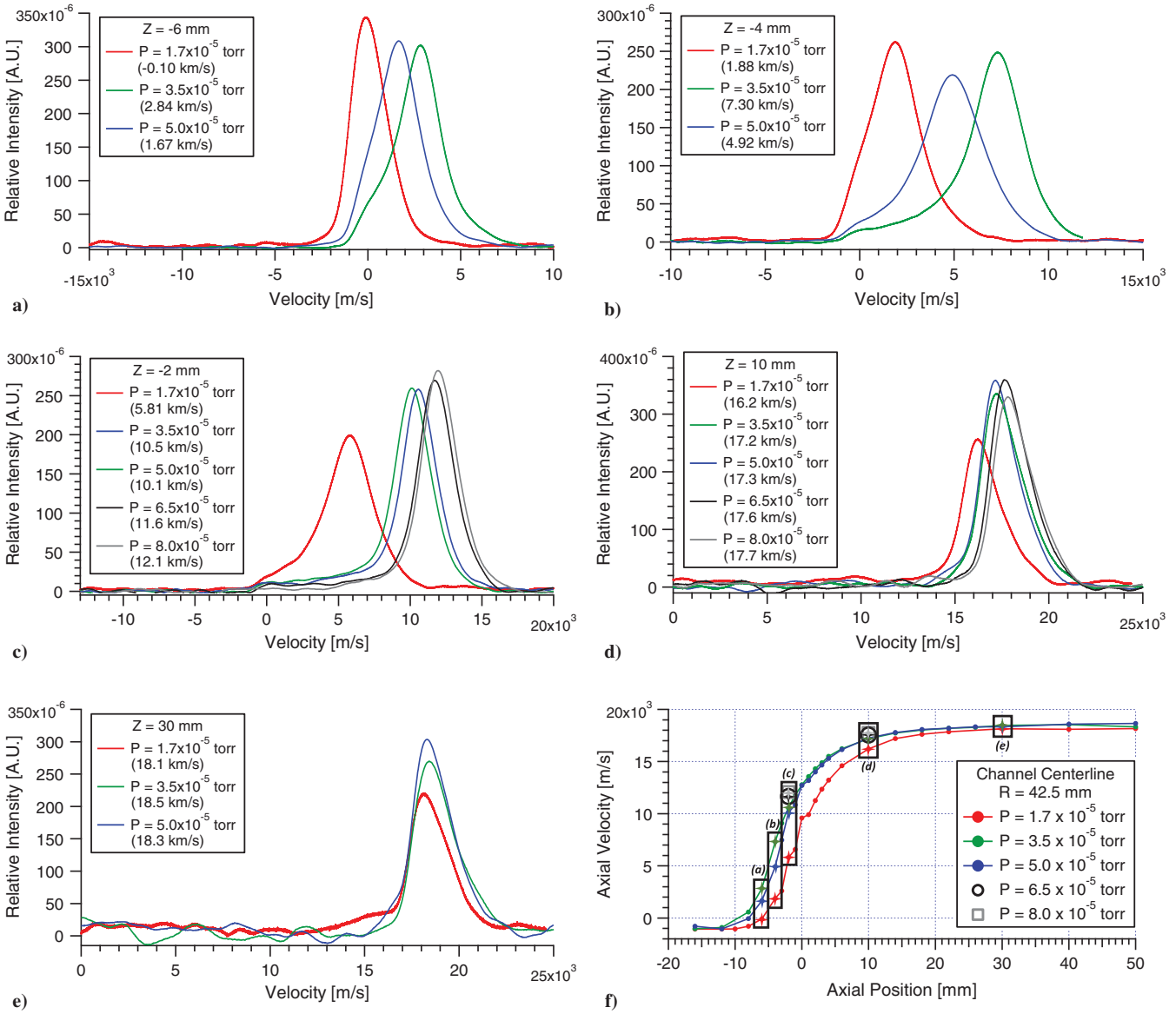

Fig. 6 Time-averaged axial IVDFs at a) $Z = -6$ mm, b) $Z = -4$ mm, c) $Z = -2$ mm, d) $Z = 10$ mm, and e) $Z = 30$ mm along the thruster discharge channel centerline. Figure 6f indicates the most probable velocities being compared in Figs. 6a–6e.

the density of xenon neutrals dipped below the facility background density from the exit plane to approximately 40 mm into the near-field plume. Highly efficient propellant utilization within the thruster channel was the primary cause of the neutral depletion. However, it was also noted that ionization mechanisms continued into the near-field plume. The neutral velocities in this study were higher than expected, implying that the diffusion of cold background gas was in part replenishing the propellant source, with the slower-moving Xe neutrals being preferentially ionized [39,40] and accelerated by local electric fields. Although the depth of neutral ingestion in the discharge chamber is generally assumed to be linear with the incident particle flux, the degree to which preferential ionization of slower background neutrals impacts the measured ion velocity within a given interrogation volume is not well quantified. The process may be nonlinear due to a combination of changes in local electron temperature and the interplay between classical partially magnetized plasma conductivity versus localized turbulent electron transport, which is not fully understood.

A subsequent paper by Hargus et al. [41] showed that, for a 600 W Hall thruster, for a 600 W Hall thruster, there were two background pressures of particular interest: first, the point at which the number density of ingested background neutrals equaled the xenon ion density (near 2×10^{-5} torr); and second at higher pressures (6×10^{-5} torr) where the background neutrals equaled the thruster neutral density. In this study, it was hypothesized that variations in background pressure do not impact thruster internal acceleration mechanisms if the density of facility background neutrals is lower than neutrals emitted from the thruster. But, at higher pressures where the densities of facility background neutrals are greater than the neutral density of the thruster, electron mobility inside the thruster channel may increase and additional ionization events may occur downstream of the exit plane.

Based on previous studies, it is estimated that the neutral density at the exit plane of the SPT-100 is approximately $10^{18}/\text{m}^3$ [42]. This would place the crossover point where facility background neutrals were approximately equal to those emitted by the thruster close to the 3.5×10^{-5} torr condition. Although there is some uncertainty in using neutral density measurements taken at a different vacuum facility and wall-mounted pressure gauges to estimate the background neutral density at the exit plane of the thruster, this correlation is worthy of further investigation because it may provide insight into the mechanism causing our observation of earlier acceleration for the 3.5×10^{-5} torr operating condition as compared to 5.0×10^{-5} torr.

Moving toward the exit plane and into the near-field plume, the IVDFs of the higher-pressure conditions begin to converge on similar shapes and peak velocities. The 1.7×10^{-5} torr condition lags behind until $Z = 30$ mm into the plume, where the IVDFs all appear similar in shape, as seen in Fig. 6e.

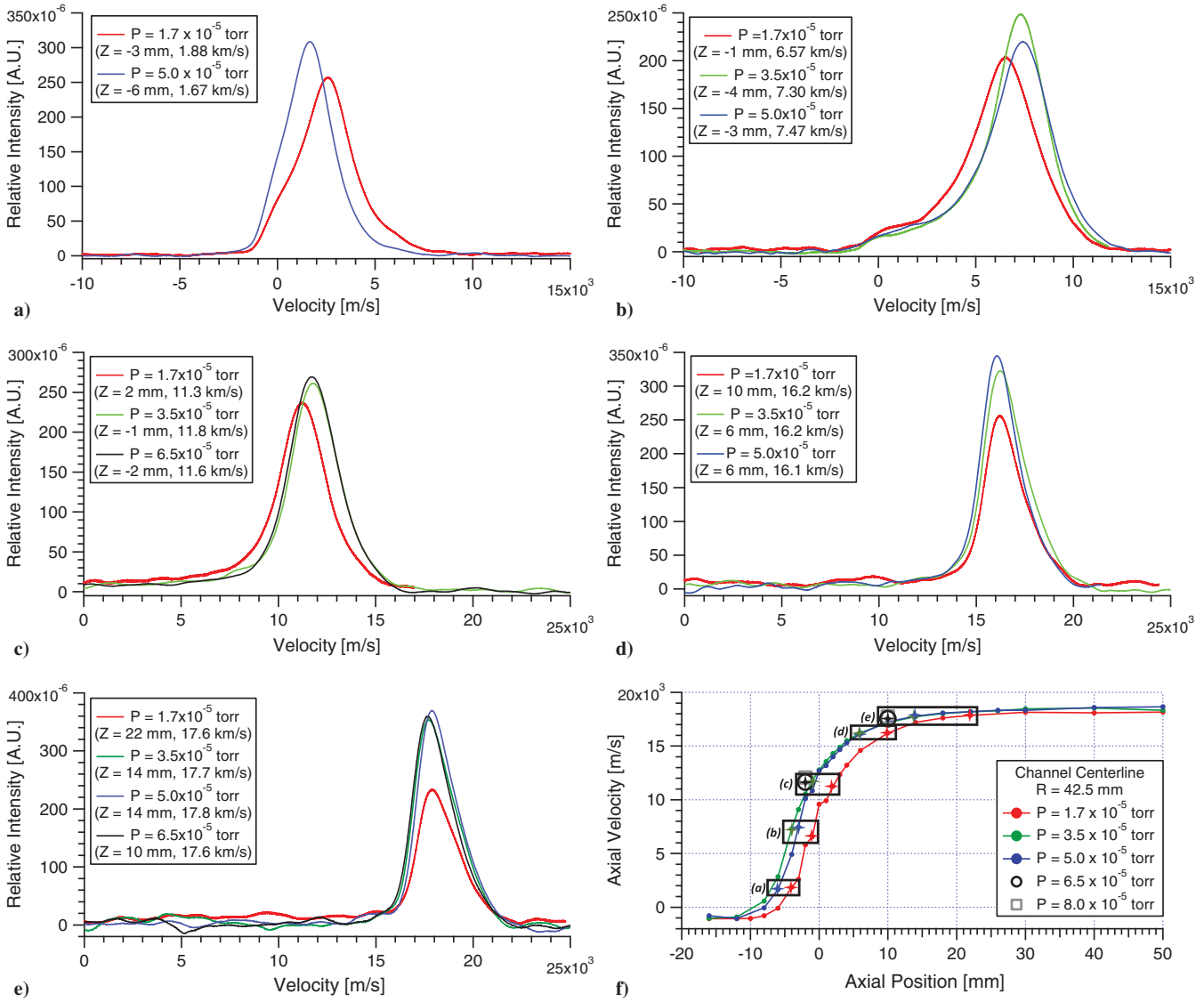

Fig. 7 Comparison of time-averaged IVDFs of similar velocity classes at varying pressures: a) 1.67–1.88 km/s, b) 6.57–7.47 km/s, c) 11.3–11.8 km/s, d) 16.1–16.2 km/s, and e) 17–6–17.7 km/s. Figure 7f indicates the most probable velocities being compared in Figs. 7a–7e.

Figure 7 provides another comparison of IVDFs at the various background pressures: this time examining the IVDFs of similar velocity class, regardless of axial position. It is interesting to note that the IVDFs in this figure appear to have similar shapes in each of the figures (Figs. 7a–7e). For example, in both traces in Fig. 7a, there is a bump in the distribution near $V = 0$ m/s and a high-velocity tail extending past $V = 5$ km/s. In Fig. 7b, all three pressure conditions have broad peaks with low-velocity tails extending to $V = 0$ m/s. And, in Figs. 7c–7e, the IVDFs narrow and approach normal distributions. This indicates that, regardless of the facility background pressure, similar acceleration mechanisms occur, but just at different axial positions.

B. Time-Resolved Measurements

Time-resolved velocity measurements were taken at axial positions from $Z = -8$ to 18 mm along the thruster channel centerline. Figure 8 shows the variation in most probable ion velocity over the course of a typical discharge current cycle for the SPT-100 operating at pressures of 1.7×10^{-5}, 3.5×10^{-5} and 5.0×10^{-5} torr. Note that the discharge current periods are shorter with increased pressure, and the acquisition of data was adjusted to be evenly spaced along the current period.

Inside the thruster channel, the most probable velocities start out relatively invariant in time at positions from the anode out to $Z = -4$ mm for the 1.7×10^{-5} torr condition or $Z = -6$ mm for the 3.5×10^{-5} and 5.0×10^{-5} torr conditions. These correspond to the positions of peak ionization seen in Fig. 4.

In subsequent positions, $Z = -2$ mm for 1.7×10^{-5} torr and $Z = -4$ mm for 3.5×10^{-5} and 5.0×10^{-5} torr; a large jump in axial velocity occurs and the most probable velocities begin to vary in time, which are correlated to the discharge current fluctuations with an amplitude on the order of ± 350 m/s. The axial positions of -2 and -4 mm correspond to the widest time-averaged IVDFs in Fig. 4. Figure 9 provides the time-resolved IVDFs for these positions. Note that the time axis is scaled in each subfigure to match the length of a typical discharge current cycle.

Each vertical slice of the color maps represents an IVDF with 1 μs time resolution at the corresponding phase of the discharge current cycle. Averaging together the time-resolved IVDFs results in an IVDF matching the time-averaged measurement. The velocities tend to increase to a maxima about one-quarter oscillation period after the discharge current peak (90 deg out of phase), and then they fall to a minima as the discharge current begins its next rampup.

Further into the near-field plume, at positions where the time-averaged IVDFs become more narrow, the temporal dependence of the most probable velocity again decreases as the axial ion velocity asymptotes to ~18.1 km/s. The exception to this trend is for $Z = 18$ mm at $P = 3.5 \times 10^{-5}$ torr, where there is a bump in velocity around 13 μs that contributes to a slight high-velocity tail in the time-averaged distribution. It is uncertain why this change is only present

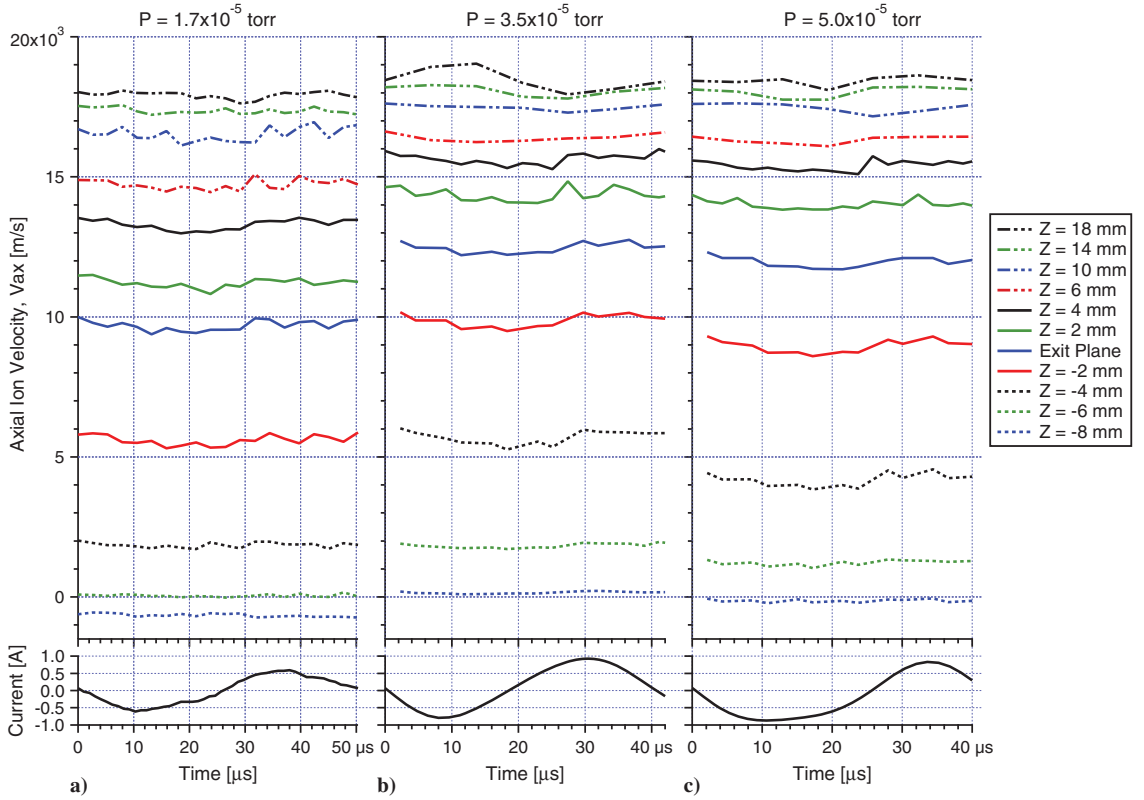

Fig. 8 Time-resolved axial ion velocities along the centerline of the discharge channel over a discharge current period at a) 1.7×10^{-5} torr, b) 3.5×10^{-5} torr, and c) 5.0×10^{-5} torr.

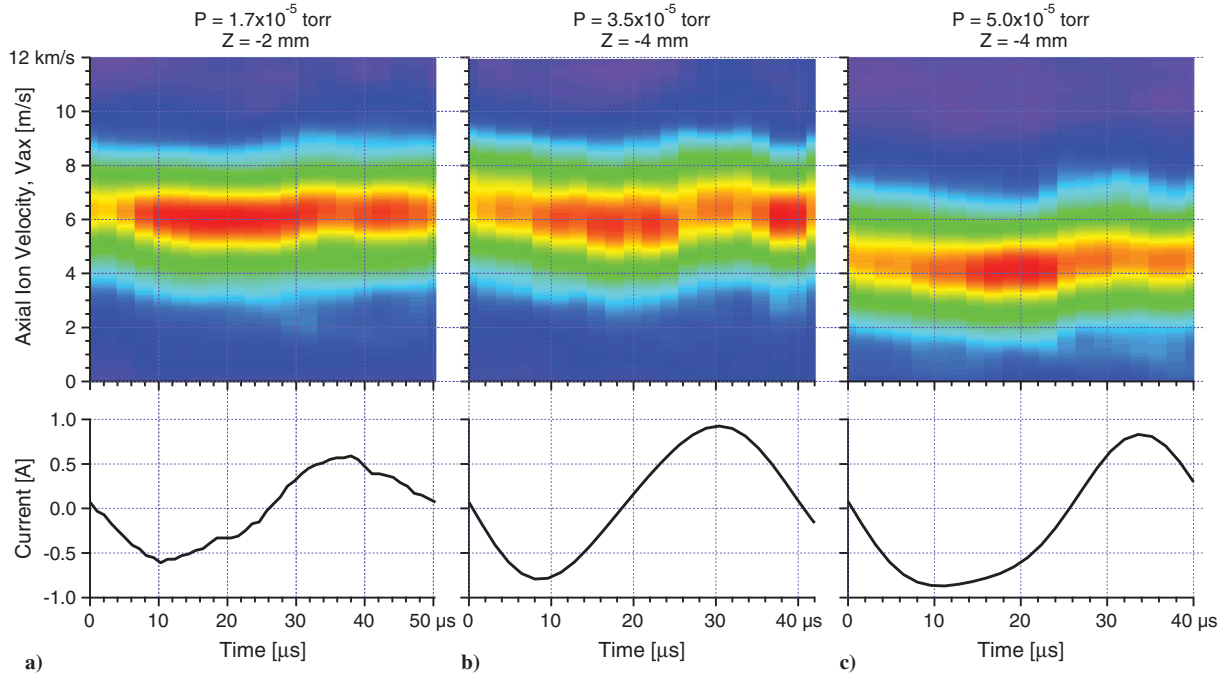

Fig. 9 Time-resolved axial ion velocities in the acceleration region of the SPT-100: a) $Z = -2$ mm, 1.7×10^{-5} torr, b) $Z = -4$ mm, 3.5×10^{-5} torr, and c) $Z = -4$ mm, 5.0×10^{-5} torr operating conditions.

at 3.5×10^{-5} torr. But, the difference between the 19.0 km/s peak at 13 μs and the 17.9 km/s trough at 27 μs is well outside the bounds of the ± 100 m/s repeatability seen in our measurements; therefore, we believe this feature to be real.

Within each spatial point, there is little variation in the fluorescence intensity with time, with the largest changes also occurring in the ionization region ($Z = -6$ to -2 mm) where the intensity is ~75% of its maximum as the discharge current decreases toward its trough, and it reaches a maximum just before the maximum in discharge current. Overall, the amplitude of the velocity oscillations and fluctuations in IVDF intensity remain consistent for varying facility background pressures. These results further emphasize that the acceleration profiles within the Hall thruster discharge channel are geometrically similar at varying background pressures but shifted in position.

Previous works on 600 W [28] and 400 W Hall thrusters [36,43] as well as a diverging cusped field thruster [44] have related the fluctuations

in ion velocity and fluorescence excitation line shape intensity to standard models of a Hall thruster breathing mode [45,46]. The discharge current increases as an ionization front moves upstream, consuming neutral propellant and increasing the population of free electrons. The fluorescence intensity consequently reaches its maximum. The newly generated ions accelerate out of the channel according to the local potential field that is also changing with time. Ions obtain their maximum velocity soon after the point of peak ionization, and the ion density (and measured intensity) falls as the ions accelerate. The ionization front moves back downstream during the discharge current trough, the neutral population builds, and eventually, the channel is left with slower ions that did not experience as large of a potential drop as the others. The cycle repeats as the discharge current ramps up again.

Although the SPT-100 appears to have similar trends to this breathing mode model, the results are not nearly as pronounced as thrusters such as the BHT-600. In the BHT-600, variations in ion velocity in the ionization region inside the channel are as large as 15 km/s over a discharge current period, with the peak intensity dropping to as low as 25% of its maximum, as opposed to the 75% seen in the SPT-100. The smaller intensity and velocity variations could, in part, be due to fluctuations in the lengths of typical discharge current periods causing sampling and averaging of nearby phases in the current cycle. Although the temporal resolution of the sample-hold method decreases as the discharge current deviates from periodic, the results provide further evidence that the mechanism for ionization and acceleration is not changing with varying facility background pressure, but it is changing in position.

IV. Conclusions

This paper presents the results of the time-averaged and time-resolved laser-induced fluorescence velocimetry of an SPT-100 Hall thruster operating at varying vacuum chamber background pressures. In general, it is hypothesized that, for the higher-pressure conditions, electron transport in the thruster discharge channel is enhanced by collisions with chamber background neutrals, pushing the ionization and acceleration regions upstream as compared to the lower-pressure conditions. This results in higher velocities inside the discharge channel that eventually converge to the same value several centimeters into the near-field plume due to ions experiencing the same total applied potential drop. This hypothesis is well supported by previous background pressure studies on other Hall thrusters.

For the SPT-100, although the ionization and acceleration regions did move upstream as expected when pressure was increased above the nominal 1.7×10^{-5} torr, the 3.5×10^{-5} torr condition jumped ahead of the 5.0×10^{-5} torr condition, with acceleration beginning ~1 mm sooner in the discharge channel. Although this anomaly is not fully understood, it is attributed to the thruster operating at a condition in which the incident flux of the facility background neutrals at 3.5×10^{-5} torr is similar to the number density of xenon neutrals emitted by the thruster. This crossover point may cause the thruster to operate in a regime in which classical partially magnetized plasma conductivity and localized turbulent electron transport interact in a nonlinear fashion. Further investigation is required to better understand the interplay between these mechanisms.

These results emphasize how difficult it is to deconvolve the effects of facility background pressure from thruster operation. Overall, it is proposed that the relative number density of the neutrals in the acceleration channel as compared to the background neutral number density at the thruster exit plane is a more meaningful parameter for determining the sensitivity of a thruster to background pressure than the measurement of pressure alone. It would therefore be important to have an accurate measurement of the neutral density or propellant utilization fraction for a thruster when determining the validity of ground test measurements and how they are extrapolated to on-orbit conditions.

Acknowledgments

This work is sponsored in part by the U.S. Air Force Office of Scientific Research, with M. Kendra as Program Manager.

References

[1] Hofer, R., Peterson, P., and Gallimore, A., "Characterizing Vacuum Facility Backpressure Effects on the Performance of a Hall Thruster," *Proceedings of the 27th International Electric Propulsion Conference*, Electric Rocket Propulsion Soc. Paper IEPC-01-045, Fairview Park, OH, Oct. 2001.

[2] Walker, M. L. R., Victor, A. L., Hofer, R. R., and Gallimore, A. D., "Effect of Backpressure on Ion Current Density Measurements in Hall Thruster Plumes," *Journal of Propulsion and Power*, Vol. 21, No. 3, May–June 2005, pp. 408–415. doi:10.2514/1.7713

[3] Nakles, M. R., and Hargus, W. A., Jr., "Background Pressure Effects on Ion Velocity Distribution Within a Medium-Power Hall Thruster," *Journal of Propulsion and Power*, Vol. 27, No. 4, 2011, pp. 737–743. doi:10.2514/1.48027

[4] Diamant, K. D., Liang, R., and Corey, R. L., "The Effect of Background Pressure on SPT-100 Hall Thruster Performance," *50th AIAA/ASME/SAE/ASEE Joint Propulsion Conference*, AIAA Paper 2014-3710, 2014. doi:10.2514/6.2014-3710

[5] Spektor, R., Tighe, W. G., and Kamhawi, H., "Laser Induced Fluorescence Measurements in a Hall Thruster as a Function of Background Pressure," *52nd AIAA/SAE/ASEE Joint Propulsion Conference and Exhibit*, AIAA Paper 2016-4624, 2016. doi:10.2514/6.2016-4624

[6] Frieman, J. D., Liu, T. M., and Walker, M. L. R., "Background Flow Model of Hall Thruster Neutral Ingestion," *Journal of Propulsion and Power*, Vol. 33, No. 5, Sept.–Oct. 2017, pp. 1087–1101. doi:10.2514/1.B36269

[7] Randolph, T., Kim, V., Kaufman, H., Kozubsky, K., Zhurin, V., and Day, M., "Facility Effects on Stationary Plasma Thruster Testing," *Proceedings of the 23rd International Electric Propulsion Conference*, Electric Rocket Propulsion Soc. Paper IEPC-1993-093, Fairview Park, OH, Sept. 2013.

[8] Kamhawi, H., Huang, W., Haag, T., and Spektor, S., "Investigation of the Effects of Facility Background Pressure on the Performance and Voltage-Current Characteristics of the High Voltage Hall Accelerator," *50th AIAA/ASME/SAE/ASEE Joint Propulsion Conference and Exhibit*, AIAA Paper 2014-3707, 2014. doi:10.2514/6.2014-3707

[9] Dankanich, J. W., Walker, M., Swiatek, M. W., and Yim, J. T., "Recommended Practice for Pressure Measurement and Calculation of Effective Pumping Speed in Electric Propulsion Testing," *Journal of Propulsion and Power*, Vol. 33, No. 3, 2017, pp. 668–680. doi:10.2514/1.B35478

[10] Myers, R., and Manzella, D., "Stationary Plasma Thruster Plume Characteristics," *Proceedings of the 23rd International Electric Propulsion Conference and Exhibit*, Electric Rocket Propulsion Soc. Paper IEPC-93-096, Fairview Park, OH, Sept. 1993.

[11] Manzella, D., and Sankovic, J., "Hall Thruster Ion Beam Characterization," *31st AIAA/ASME/SAE/ASEE Joint Propulsion Conference*, AIAA Paper 1995-2927, 1995. doi:10.2514/6.1995-2927

[12] Lebedev, U., Popov, G., and Zhurin, V., "Measurement of Plasma Parameters in the Stationary Plasma Thruster (SPT-100) Plume and its Effect on Spacecraft Components," *28th Joint Propulsion Conference and Exhibit*, AIAA Paper 1992-3156, 1992. doi:10.2514/6.1992-3156

[13] Pencil, E., "Preliminary Far-Field Plume Sputtering of the Stationary Plasma Thruster (SPT-100)," *Proceedings of the 23rd International Electric Propulsion Conference and Exhibit*, Electric Rocket Propulsion Soc. Paper IEPC-93-098, Fairview Park, OH, Sept. 1993.

[14] Pencil, E., Randolph, T., and Manzella, D., "End-of-Life Stationary Plasma Thruster Far-Field Plume Characterization," *32nd AIAA/ASME/SAE/ASEE Joint Propulsion Conference*, AIAA Paper 1996-2709, 1996. doi:10.2514/6.1996-2709

[15] Manzella, D., "Stationary Plasma Thruster Plume Emissions," *Proceedings of the 23rd International Electric Propulsion Conference and Exhibit*, Electric Rocket Propulsion Soc. Paper IEPC-93-097, Fairview Park, OH, Sept. 1993.

[16] Manzella, D., "Stationary Plasma Thruster Ion Velocity Distribution," *30th AIAA/ASME/SAE/ASEE Joint Propulsion Conference*, AIAA Paper 1994-3141, 1994. doi:10.2514/6.1994-3141

[17] MacDonald-Tenenbaum, N., Pratt, Q., Nakles, M., Pilgram, N., and Hargus, W., Jr., "Ion Velocity Distributions in an SPT-100 Hall Thruster," *Proceedings of the 35th International Electric Propulsion Conference and*

Exhibit, Electric Rocket Propulsion Soc. Paper IEPC-2017-132, Fairview Park, OH, Oct. 2017.

[18] Brown, D. L., and Gallimore, A. D., "Evaluation of Facility Effects on Ion Migration in a Hall Thruster Plume," *Journal of Propulsion and Power*, Vol. 27, No. 3, May–June 2011, pp. 573–585. doi:10.2514/1.B34068

[19] Hansen, J. E., and Persson, W., "Revised Analysis of Singly Ionized Xenon, Xe II," *Physica Scripta*, Vol. 36, No. 4, 1987, pp. 602–643. doi:10.1088/0031-8949/36/4/005

[20] Nakles, M. R., Hargus, W. A., Jr., Delgado, J. J., and Corey, R. L., "A Performance Comparison of Xenon and Krypton Propellant on an SPT-100 Hall Thruster," *Proceedings of the 32nd International Electric Propulsion Conference and Exhibit*, Electric Rocket Propulsion Soc. Paper IEPC-2011-003, Fairview Park, OH, Sept. 2011.

[21] Huang, W., Kamhawi, H., Lobbia, R., and Brown, D., "Effect of Background Pressure on the Plasma Oscillation Characteristics of the HiVHAc Hall Thruster," *50th AIAA/ASME/SAE/ASEE Joint Propulsion Conference*, AIAA Paper 2014-3708, 2014. doi:10.2514/6.2014-3708

[22] Hargus, W. A., Jr., and Cappelli, M. A., "Laser-Induced Fluorescence Measurements of Velocity Within a Hall Discharge," *Applied Physics B*, Vol. 72, No. 8, 2001, pp. 961–969. doi:10.1007/s003400100589

[23] Mazouffre, S., Gawron, D., Kulaev, V., and Sadehgi, N., "Xe^+ Ion Transport in the Crossed-Field Discharge of a 5-kW-Class Hall Effect Thruster," *IEEE Transactions on Plasma Science*, Vol. 36, No. 5, 2008, pp. 1967–1976. doi:10.1109/TPS.2008.2004240

[24] MacDonald, N. A., Young, C. V., Cappelli, M. A., and Hargus, W. A., Jr., "Ion Velocity and Plasma Potential Measurements of a Cylindrical Cusped Field Thruster," *Journal of Applied Physics*, Vol. 11, No. 9, 2012, Paper 093303. doi:10.1063/1.4707953

[25] Hargus, W. A., Jr., and Nakles, M. R., "Ion Velocity Measurements Within the Acceleration Channel of a Low-Power Hall Thruster," *IEEE Transactions on Plasma Science*, Vol. 36, No. 5, 2008, pp. 1989–1997. doi:10.1109/TPS.2008.2003967

[26] Miller, M. H., Roig, R. A., and Bengtson, R. D., "Transition Probabilities of Xe I and Xe II," *Physical Review A: General Physics*, Vol. 8, No. 1, 1973, pp. 480–486. doi:10.1103/PhysRevA.8.480

[27] Kramida, A., Ralchenko, Y., and Reader, J., *NIST Atomic Spectra Database* [online database], Ver. 5.2, National Inst. of Standards and Technology, Gaithersburg, MD, 2014, http://physics.nist.gov/asd [retrieved 15 May 2015].

[28] MacDonald-Tenenbaum, N., Young, C., Lucca Fabris, A., Nakles, M., Hargus, W., Jr., and Cappelli, M., "Time-Synchronized Continuous Wave Laser Induced Fluorescence Velocity Measurements of a 600 Watt Hall Thruster," *Proceedings of the 34th International Electric Propulsion Conference*, Electric Rocket Propulsion Soc. Paper IEPC 2015-350, Fairview Park, OH, July 2015.

[29] MacDonald, N. A., Cappelli, M. A., and Hargus, W. A., Jr., "Time-Synchronized Continuous Wave Laser-Induced Fluorescence on an Oscillatory Xenon Discharge," *Review of Scientific Instruments*, Vol. 83, No. 11, 2012, Paper 113506. doi:10.1063/1.4766958

[30] Lucca Fabris, A., Young, C. V., and Cappelli, M. A., "Excited State Population Dynamics of a Xenon AC Discharge," *Plasma Sources Science and Technology*, Vol. 24, No. 5, 2015, Paper 055013. doi:10.1088/0963-0252/24/5/055013

[31] Young, C. V., "Dynamics of Plasma Discharges used for Space Propulsion," Ph.D. Dissertation, Mechanical Engineering Dept., Stanford Univ., Stanford, CA, 2016, pp. 169–177.

[32] Hargus, W. A., Jr., and Nakles, M. R., "Evolution of the Ion Velocity Distribution in the Near Field of the BHT-200-X3 Hall Thruster," *42nd AIAA/ASME/SAE/ASEE Joint Propulsion Conference and Exhibit*, AIAA Paper 2006-4991, 2006. doi:10.2514/6.2006-4991

[33] Lucca Fabris, A., Young, C. V., and Cappelli, M. A., "Time-Resolved Laser-Induced Fluorescence Measurement of Ion and Neutral Dynamics in a Hall Thruster During Ionization Oscillations," *Journal of Applied Physics*, Vol. 118, No. 23, 2015, Paper 233301. doi:10.1063/1.4937272

[34] Scharfe, M. K., Gascon, N., and Cappelli, M. A., "Comparison of Hybrid Hall Thruster Model to Experimental Measurements," *Physics of Plasmas*, Vol. 13, No. 8, 2006, Paper 083505. doi:10.1063/1.2336186

[35] Parra, F., Ahedo, E., Fife, J., and Martinez-Sanchez, M., "A Two-Dimensional Hybrid Model of the Hall Thruster Discharge," *Journal of Applied Physics*, Vol. 100, No. 2, 2006, Paper 023304. doi:10.1063/1.2219165

[36] Young, C. V., Lucca Fabris, A., and Cappelli, M. A., "Ion Dynamics in an ExB Hall Plasma Accelerator," *Applied Physics Letters*, Vol. 106, No. 4, 2015, Paper 044102. doi:10.1063/1.4907283

[37] Boyd, I. D., "Review of Hall Thruster Plume Modeling," *Journal of Spacecraft and Rockets*, Vol. 38, No. 3, 2001, pp. 381–387. doi:10.2514/2.3695

[38] Crofton, M., Hsu Schouten, A., Young, J., Beiting, E., Diamant, K., Corey, R., and Delgado, J., "Neutral Xenon Density in the SPT-140 Near-Field Plume," *Proceedings of the 33rd International Electric Propulsion Conference*, Electric Rocket Propulsion Soc. Paper IEPC 2013-399, Fairview Park, OH, Oct. 2013.

[39] Hargus, W. A., Jr., and Cappelli, M. A., "Laser-Induced Fluorescence Measurements of Velocity Within a Hall Discharge," *Applied Physics B*, Vol. 72, No. 8, 2001, pp. 961–969. doi:10.1007/s003400100589

[40] Mazouffre, S., Bourgeois, G., Garrigues, L., and Pawelec, E., "A Comprehensive Study on the Atom Flow in the Cross-Field Discharge of a Hall Thruster," *Journal of Physics D: Applied Physics*, Vol. 44, No. 10, 2011, Paper 105203. doi:10.1088/0022-3727/44/10/105203-3727

[41] Hargus, W. A., Jr., Tango, L. J., and Nakles, M. R., "Background Pressure Effects on Krypton Hall Effect Thruster Internal Acceleration," *Proceedings of the 33rd International Electric Propulsion Conference*, Electric Rocket Propulsion Soc. Paper IEPC 2013-340, Fairview Park, OH, Oct. 2013.

[42] Boyd, I., "Hall Thruster Far Field Plume Modeling and Comparison to Express Flight Data," *40th AIAA Aerospace Sciences Meeting and Exhibit*, AIAA Paper 2002-0487, 2002. doi:10.2514/6.2002-388

[43] Lucca Fabris, A., Young, C. V., and Cappelli, M. A., "Time-Resolved Laser-Induced Fluorescence Measurement of Ion and Neutral Dynamics in a Hall Thruster During Ionization Oscillations," *Journal of Applied Physics*, Vol. 118, No. 23, 2015, Paper 233301. doi:10.1063/1.4937272

[44] MacDonald, N. A., Cappelli, M. A., and Hargus, W. A., Jr., "Time-Synchronized Continuous Wave Laser-Induced Fluorescence Axial Velocity Measurements in a Diverging Cusped Field Thruster," *Journal of Physics D: Applied Physics*, Vol. 47, No. 11, 2014, Paper 115204. doi:10.1088/0022-3727/47/11/115204

[45] Boeuf, J. P., and Garrigues, L., "Low Frequency Oscillations in a Stationary Plasma Thruster," *Journal of Applied Physics*, Vol. 84, No. 7, 1998, pp. 3541–3554. doi:10.1063/1.368529

[46] Barral, S., and Ahedo, E., "Low-Frequency Model of Breathing Oscillations in Hall Discharges," *Physical Review E*, Vol. 79, No. 4, 2009, Paper 046401. doi:10.1103/PhysRevE.79.046401

L. B. King
Associate Editor